PERGAMON

Electrochimica Acta 46 (2001) 897–906

ELECTROCHIMICA Acta

www.elsevier.nl/locate/electacta

Mechanisms of lithium transport through transition metal oxides studied by analysis of current transients

Heon-Cheol Shin, Su-Il Pyun *, Sung-Woo Kim, Min-Hyung Lee

Department of Materials Science and Engineering, Korea Advanced Institute of Science and Technology, 373-1 Kusong-Dong, Yusong-Gu, Taejon 305-701, South Korea

Received 29 June 2000

Abstract

Lithium transport through such transition metal oxides as $Li_{1+\delta}[Ti_{5/3}Li_{1/3}]O_4$, $Li_{1-\delta}NiO_2$ and $Li_\delta V_2O_5$ was investigated by analysis of current transients. All the experimental current transients in shape deviated markedly from the Cottrell character during the whole intercalation/deintercalation, and the initial current level varied linearly with the applied potential step according to Ohm's law. Moreover, it was observed that the current transient during phase transformation is characterised by a 'current plateau'. The current transient was simulated as a function of applied potential by numerical analysis assuming 'cell-impedance-controlled' lithium transport. The numerically simulated current transient featured quantitative behaviour characteristic of non-Cottrell behaviour and exhibited a 'current plateau'. The lithium transport mechanism through the oxides is discussed in terms of 'cell-impedance-controlled' intercalation/deintercalation.

Keywords: Current transient; Cell-impedance; $LiNiO_2$; $Li_{4/3}Ti_{5/3}O_4$; V_2O_5

1. Introduction

Electrochemical intercalation of lithium into transition metal oxides has been extensively studied for applications as cathodes in rechargeable lithium batteries and in electrochromic displays [1–5]. Over the last two decades, most research on lithium intercalation has been focused on the diffusion of lithium within the oxide, assuming that this is the rate-controlling process of the intercalation reaction [6,7].

In earlier communications from our laboratory on the analysis of experimental and theoretical current transients, however, it has been reported that 'cell-impedance' crucially determines the value and shape of current transients during lithium intercalation into and deintercalation from $Li_{1-\delta}CoO_2$ composite [8] and thin film [9] electrodes. Moreover, it has been suggested that lithium ions at the electrode/electrolyte interface are subject to an 'apparent' potentiostatic boundary condition rather than the 'real' potentiostatic boundary condition. Under the circumstances, we need to explore lithium transport through intercalation compounds other than $Li_{1-\delta}CoO_2$, and then to re-examine whether or not lithium intercalation into these compounds during potential stepping is still limited by lithium diffusion through the electrode subjected to the 'real' potentiostatic boundary condition, i.e. whether or not the Cottrell relation describes the current transients.

This work is aimed at elucidating the lithium transport mechanisms through such lithium intercalation compounds as $Li_{1+\delta}[Ti_{5/3}Li_{1/3}]O_4$, $Li_{1-\delta}NiO_2$ and $Li_\delta V_2O_5$. For this purpose open-circuit potential transients and potentiostatic current transients were measured on the oxide electrodes as functions of lithium

* Corresponding author. Tel.: +82-42-869 3319; fax: +82-42-869 3310.

E-mail address: sipyun@mail.kaist.ac.kr (S.-I. Pyun).

0013-4686/01/$ - see front matter
PII: S0013-4686(00)00676-9

stoichiometry and applied potential respectively. The current transients have been simulated as a function of applied potential by taking the assumption that lithium intercalation/deintercalation is limited by 'cell-impedance' and compared with those determined experimentally.

2. Experimental

The $Li_{1+\delta}[Ti_{5/3}Li_{1/3}]O_4$ [10], $Li_{1-\delta}NiO_2$ [11] and $Li_\delta V_2O_5$ [12] electrode specimens were prepared as described previously. A three-electrode electrochemical cell was employed for the electrochemical measurements. The reference and counter electrodes were constructed from lithium foil (Foote Mineral Co. USA, purity 99.9%), and a 1 M solution of $LiClO_4$ in propylene carbonate (PC) was used as the electrolyte.

The galvanostatic charge–discharge and galvanostatic intermittent charge–discharge experiments were conducted by using a Solartron 1287 Electrochemical Interface. The charge and discharge currents were selected so that a change in lithium content of $\Delta\delta = 1$ for $Li_{1+\delta}[Ti_{5/3}Li_{1/3}]O_4$, $Li_{1-\delta}NiO_2$ and $Li_\delta V_2O_5$ would occur for 5 or 10 h. The deviation δ from the ideal stoichiometry ($\delta = 0$) was calculated from the values of the mass of the oxide and of the total electrical charge that was transferred during the whole charge–discharge cycle.

The potentiostatic current transient experiment was performed by application of large potential steps. The current transients were measured on the carbon-dispersed composite electrodes by dropping/jumping one potential to the other lithium injection/extraction potentials. Prior to lithium injection/extraction, the electrode was maintained at the initial potential for a sufficiently long time to obtain a low steady-state current.

All the electrochemical experiments were performed at 25°C in a glove box (MECAPLEX GB94) filled with purified argon gas.

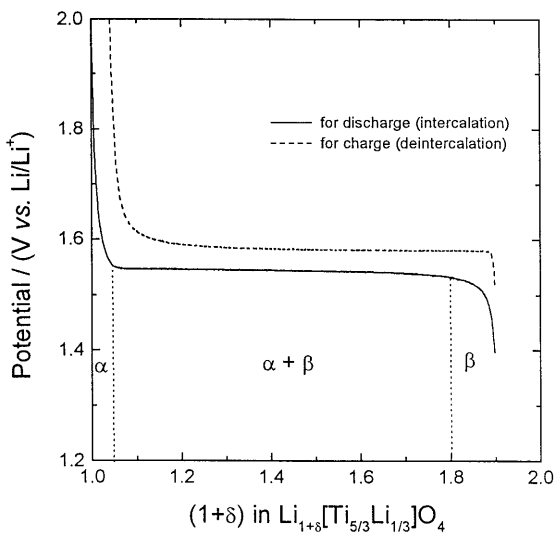

Fig. 1. The galvanostatic charge–discharge curve obtained from the cell of Li/1 M $LiClO_4$–PC solution/$Li_{1+\delta}[Ti_{5/3}Li_{1/3}]O_4$. The change in lithium content, $\Delta\delta = 1$, occurs over 5 h.

3. Results and discussion

3.1. $Li_{1+\delta}[Ti_{5/3}Li_{1/3}]O_4$ electrode

Fig. 1 gives the galvanostatic charge–discharge curve obtained from the carbon-dispersed $Li_{1+\delta}[Ti_{5/3}Li_{1/3}]O_4$ composite electrode in 1 M $LiClO_4$–PC solution as a function of intercalated lithium content. In the present work, all the galvanostatic charge–discharge curves and potentiostatic current transients were measured on the electrodes that previously had undergone at least one cycle of charge–discharge in order to eliminate the effect of the initial irreversible capacity on both charge–discharge curves and current transients. The discharge curve was characterised by an extremely flat potential of 1.56 V versus Li/Li^+, which was almost equal to the plateau potential in the open-circuit voltage (OCV) curve [13].

The occurrence of a 'potential plateau' is generally agreed from a thermodynamic viewpoint to be caused by the coexistence of two different compositional or structural phases. Several researchers have found from X-ray diffractometry that the structure of $Li_{1+\delta}[Ti_{5/3}Li_{1/3}]O_4$ is unchanged as lithium intercalation proceeds [13,14]. So, it seems to be reasonable to ascribe the plateau at 1.56 V versus Li/Li^+ to the coexistence of an Li-poor α phase and an Li-rich β phase.

First, to follow lithium transport kinetically through a single phase of $Li_{1+\delta}[Ti_{5/3}Li_{1/3}]O_4$, the cathodic and anodic current transients were measured in 1 M $LiClO_4$–PC solution at the potential drop and potential jump respectively between applied potentials higher than the plateau potential [8]. The results are plotted on a logarithmic scale in Fig. 2. The absolute values of the slopes of all the logarithmic current transients increased monotonically with time during the whole intercalation/deintercalation; the linear relationship (the Cottrell behaviour) was never followed. Moreover, the cathodic current transients at the potential steps from 1.700 to 1.650, 1.700 to 1.600, and 1.700 to 1.575 V versus Li/Li^+ intersected those anodic transients from 1.650 to 1.700, 1.600 to 1.700, and 1.575 to 1.700 V versus Li/Li^+ respectively.

This abnormal lithium transport behaviour, which includes the intersection and the non-Cottrell characters of the current transients, was quite similar to that

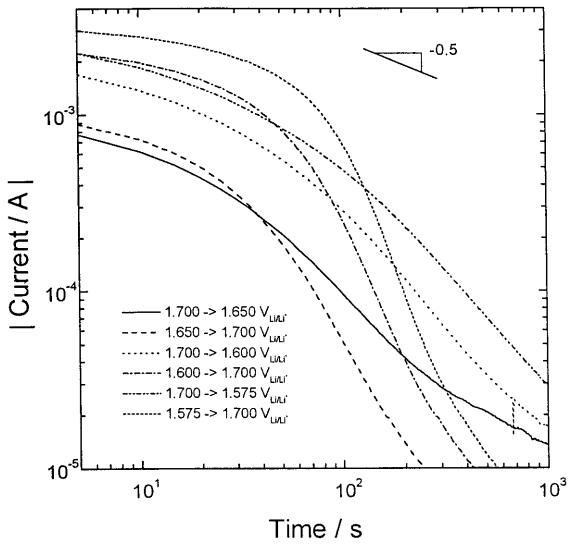

Fig. 2. The cathodic and anodic current transients, obtained experimentally from the $Li_{1+\delta}[Ti_{5/3}Li_{1/3}]O_4$ electrode in 1 M $LiClO_4$–PC solution at the potential drop and potential jump respectively, between applied potentials higher than the plateau potential.

observed in the preceding work on lithium transport kinetics of $Li_{1-\delta}CoO_2$ [8]. In that work, it was strongly suggested that the anomalous current transient is responsible for 'cell-impedance-controlled' lithium transport, and that the interface between the electrode and the electrolyte is subjected to the 'apparent' potentiostatic boundary condition rather than the 'real' potentiostatic boundary condition. From the significant similarity of lithium transport behaviours through $Li_{1-\delta}CoO_2$ and through $Li_{1+\delta}[Ti_{5/3}Li_{1/3}]O_4$, it is conceivable that lithium intercalation into and deintercalation from the single-phase $Li_{1+\delta}[Ti_{5/3}Li_{1/3}]O_4$ are governed by 'cell-impedance'. By 'cell-impedance' we mean the internal cell resistance, major sources of which may be the bulk electrolyte, the electrolyte/electrode interface region, and the bulk electrode [15,16].

Next, in order to investigate lithium transport through the $Li_{1+\delta}[Ti_{5/3}Li_{1/3}]O_4$ coexisting as two phases, we made the applied potential steps encounter the plateau potential. The resulting cathodic current transients are shown on a logarithmic scale in Fig. 3(a) along with three cathodic transients obtained in the single-phase region. The current transients below the plateau potential exhibited a three-stage behaviour. The logarithmic current decreased slowly at first, then remained constant and finally decayed steeply.

It should be noted that the cathodic charge consumed during the 'current plateau' interval in the current transient was nearly equal to that during the 'potential plateau' interval in the discharge curve (Fig. 1), irrespective of the magnitude of the applied potential drop. Keeping in mind that 'current plateau' implies a constant driving force for lithium intercalation, it is unlikely that phase transformation of α to β is governed by 'diffusion-controlled' lithium transport through the electrode imposed by the 'real' potentiostatic boundary condition at the surface [8]. Rather, these situations indicate that phase transformation of α to β occurs under the 'cell-impedance-controlled' constraint, where the current delivered is determined by the difference between the electrode potential E and the applied potential E_{app}, divided by 'cell-impedance' R_{cell}.

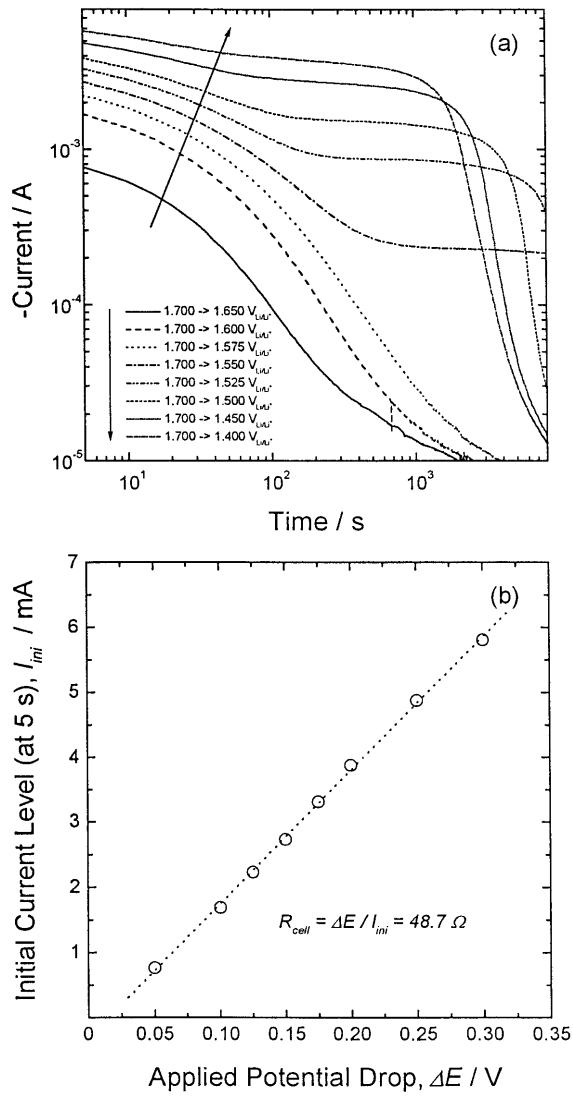

Fig. 3. (a) The cathodic current transients obtained experimentally from the $Li_{1+\delta}[Ti_{5/3}Li_{1/3}]O_4$ electrode in 1 M $LiClO_4$–PC solution at the potential drops from 1.700 V versus Li/Li^+ to various lithium injection potentials; (b) the dependence of initial current level on applied potential drop.

It is also noted that the initial current level in Fig. 3(a) is linearly proportional to the applied potential drop, as can be seen in Fig. 3(b), viz. the initial current–potential relation follows Ohm's law. This result is consistent with the above suggestion that lithium transport through the $Li_{1+\delta}[Ti_{5/3}Li_{1/3}]O_4$ in the presence of a single phase proceeds under the 'cell-impedance-controlled' constraint.

In view of these circumstances, we modelled the current transient under the assumption of 'cell-impedance-controlled' lithium transport. Since the spinel structure has a three-dimensional diffusion path and the individual oxide particles of the electrode were observed from scanning electron microscopy (SEM) to be almost spherical in shape, we selected the constituent particle of spherical symmetry for theoretical calculation.

The governing equation is Fick's diffusion equation for sphere, where diffusion was assumed to be everywhere radial [17]. The initial condition (I.C.) and the boundary condition (B.C.) are given as

$$\text{I.C.: } c = c_0 \text{ for } 0 \le r \le R^* \text{ at } t = 0 \quad (1)$$

$$\text{B.C.: } -zFA_{ea}\tilde{D}_{Li^+}\frac{\partial c}{\partial r} = \frac{E_{app} - E}{R_{cell}}$$

('cell-impedance-controlled' constraint) (2)

for $r = R^*$ at $t > 0$

$$-zFA_{ea}\tilde{D}_{Li^+}\frac{\partial c}{\partial r} = 0 \text{ (impermeable constraint)}$$

for $r = 0$ at $t \ge 0$ (3)

where c is local concentration of lithium ion, z is the valence number, F is the Faraday constant, A_{ea} is the electrochemically active area, $\tilde{D}_{Li^+}$ is the concentration-independent chemical diffusivity of lithium ion, r is the distance from the centre of the oxide particle and R^* represents the average radius of the particle.

'Cell-impedance' R_{cell} was determined to be 48.7 Ω from Fig. 3(b), and the average radius of oxide particle R^* was estimated to be ca 1 μm from SEM. The chemical diffusivity of lithium ion $\tilde{D}_{Li^+}$ was taken as 2×10^{-8} cm^2 s^{-1} from the earlier investigation [18]. Finally, the electrochemically active area A_{ea} was calculated under the assumption that A_{ea} is identical to the total surface area of the electrode comprised of the spherical particles [19], to be 197 cm^2 from the average radius R^* and the theoretical density of the oxide particles considered.

As a matter of fact, A_{ea} was overestimated on account of intimate contacts between oxide particles and conducting or binder materials, and between the oxide particles themselves [12]. In the case of the layered oxides, which will be dealt with in the following sections, the highly anisotropic layered property of the oxide additionally reduces the effective surface area for lithium intercalation. The fact that $\tilde{D}_{Li^+}$ is a strong function of A_{ea} [19], makes it much more difficult quantitatively to analyse current transients. However, fortunately in the case of our 'cell-impedance-controlled' lithium transport, it was found that the variation of $\tilde{D}_{Li^+}$ in the range of one or two order(s) in magnitude does not crucially affect the current transients in value and shape.

The functional expression $E = f(1-\delta)$ for the change in the electrode potential E with stoichiometry $1-\delta$ was first obtained from the polynomial regression analysis of the charge–discharge curve in Fig. 1. Next, we simulated the current transient assuming that lithium transport through the electrode is purely governed by 'cell impedance'. Fig. 4(a) depicts on a logarithmic scale the cathodic and anodic current transients at the potential drop and jump respectively between applied potentials higher than the plateau potential, determined from the numerical solution to Fick's diffusion equations for the conditions of Eqs. (1)–(3) by taking the values described above.

The calculated current transients (Fig. 4(a)) matched almost exactly those experimental current transients (Fig. 2) in value and shape, with regard to the non-Cottrell lithium transport behaviour and a mutual intersection of the cathodic current transient with the anodic current transient. The theoretical cathodic current transients at the potential drops of 1.700 V versus Li/Li$^+$ to various lithium injection potentials below the plateau potential (Fig. 4(b)) displayed the same three-stage character as the experimental current transients (Fig. 3(a)), and are quantitatively in good accordance with Fig. 3(a).

These results strongly indicate that lithium transport through the $Li_{1+\delta}[Ti_{5/3}Li_{1/3}]O_4$ composite electrode in 1 M $LiClO_4$–PC solution is governed by the 'cell-impedance-controlled' constraint during the whole intercalation/deintercalation. Now we should mention several factors here affecting the B.C. represented by Eq. (2) that determines the current transient in value and shape. They are for instance the variation of diffusivity and 'cell-impedance' with lithium stoichiometry, the size distribution of the oxide particles, the change in the actual applied potential step due to the tortuosity of the ionic path inside the composite electrode and the overestimated electrochemically active area, which have usually been disregarded until now.

It should be additionally stressed that 'diffusion-controlled' current transients theoretically calculated for an electrode of spherical or cylindrical symmetry can diverge slightly from the transients specified by Cottrell character within a dispersion range originating from the three different geometrical configurations of the electrode [20]. However, in fact they depart so strongly

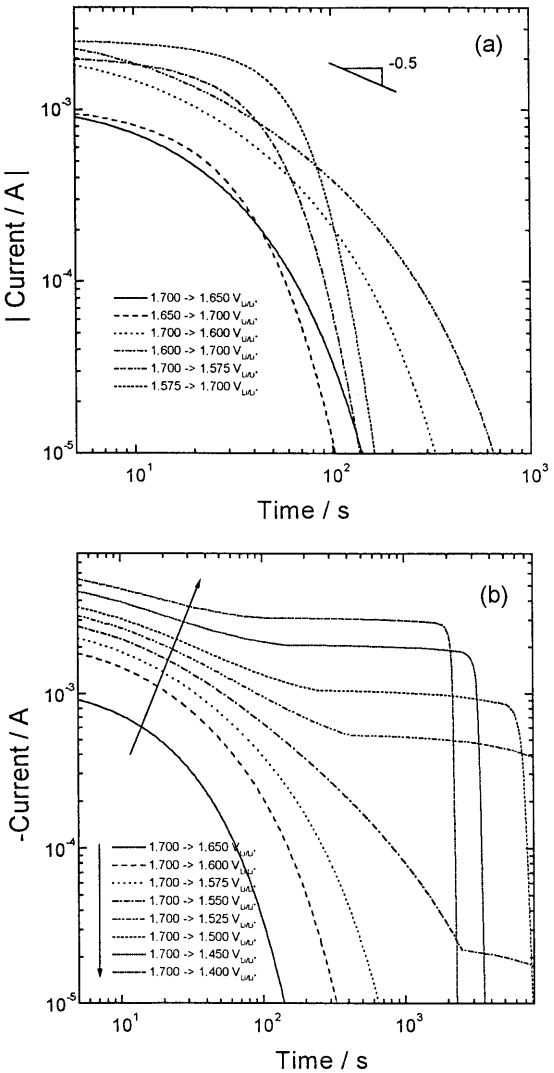

Fig. 4. (a) The cathodic and anodic current transients at the potential drop and potential jump respectively between applied potentials higher than the plateau potential and (b) the cathodic current transients at potential drops from 1.700 V versus Li/Li^+ to various lithium injection potentials, determined theoretically by numerical analysis based upon the 'cell-impedance-controlled' constraint at the interface between the electrolyte and the electrode of spherical symmetry, and the impermeable constraint at the centre of the spherical particle of the electrode.

from the experimental current transients that the former theoretical transients do not coincide with the latter experimental transients at all.

The chemical diffusivity of lithium in the electrode has usually been determined quantitatively by means of fitting the experimental current transient to various theoretical equations [17,20], which were derived assuming 'diffusion-controlled' lithium transport. In view of the above argument, however, it can be stated that this fitting method is not appropriate to provide a reliable value of lithium diffusivity in the $Li_{1+\delta}[Ti_{5/3}Li_{1/3}]O_4$ electrode in 1 M $LiClO_4$–PC solution.

3.2. $Li_{1-\delta}NiO_2$ electrode

Fig. 5 demonstrates the electrode potentials obtained from the intermittent galvanostatic charge–discharge curve of the carbon-dispersed $Li_{1-\delta}NiO_2$ composite electrode in 1 M $LiClO_4$–PC solution as a function of intercalated lithium content. The electrode potential curve displayed two 'potential plateaux' near 3.65 V and 4.02 V versus Li/Li^+, which proved to stem from the equilibrium coexistences of the first hexagonal phase and the monoclinic phase, and the monoclinic phase and the second hexagonal phase respectively [21].

Fig. 6(a) presents on a logarithmic scale the cathodic current transients obtained experimentally from the $Li_{1-\delta}NiO_2$ composite electrode in 1 M $LiClO_4$–PC solution at the potential drops from 4.0 V versus Li/Li^+ to various lithium injection potentials as indicated in the figure. The current transients did not exhibit Cottrell behaviour during the whole lithium intercalation. In addition, the initial current level is linearly proportional to the applied potential drop, as can be seen in Fig. 6(b). This result signifies that lithium transport is controlled by 'cell impedance'.

Now, let us theoretically consider 'cell-impedance-controlled' lithium transport through the $Li_{1-\delta}NiO_2$ electrode. The presence of a two-dimensional diffusion path in the layered structured oxide particle made us

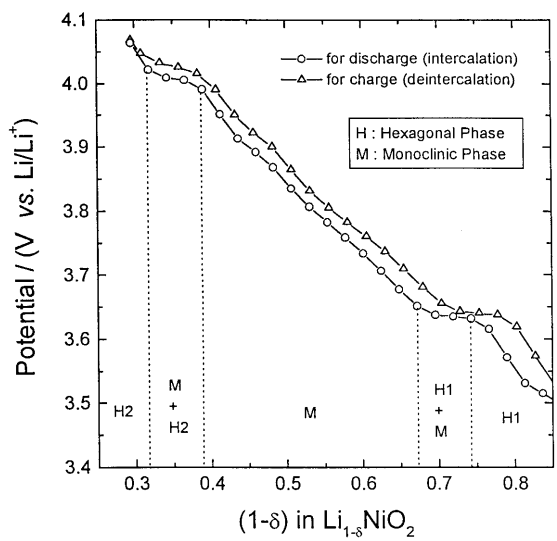

Fig. 5. The intermittent galvanostatic charge–discharge curve obtained from the cell of Li/1 M $LiClO_4$–PC solution/$Li_{1-\delta}NiO_2$. The change in lithium content, $\Delta\delta = 1$, occurs over 10 h.

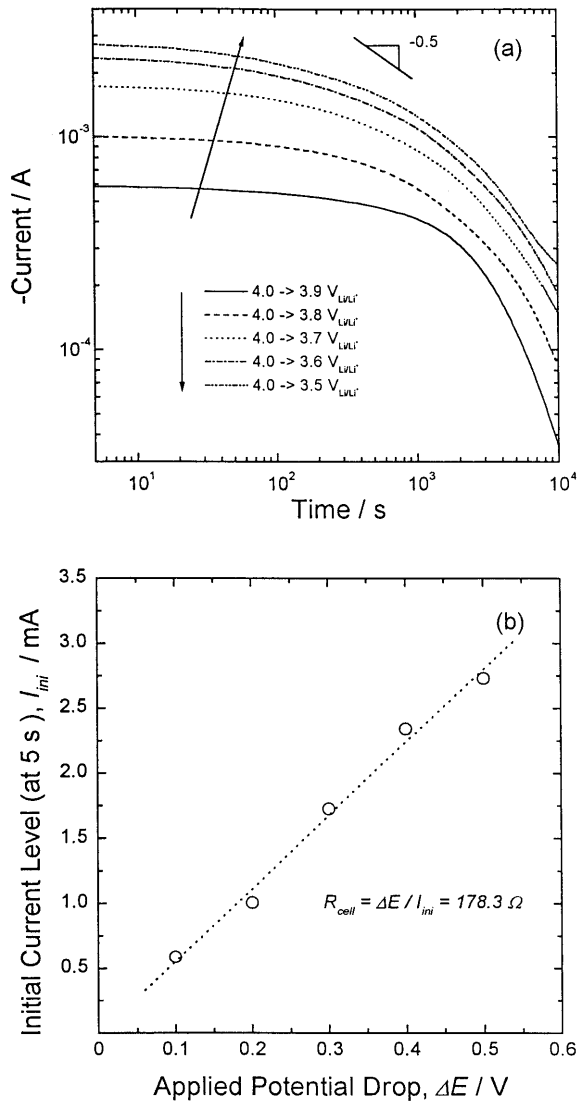

Fig. 6. (a) The cathodic current transients obtained experimentally from the $Li_{1-\delta}NiO_2$ electrode in 1 M $LiClO_4$–PC solution at the potential drops from 4.0 V versus Li/Li^+ to various lithium injection potentials, and (b) the dependence of initial current level on applied potential drop.

select the constituent particle of cylindrical symmetry for theoretical calculation. The 'cell impedance' R_{cell} and the average radius of oxide particle R^* were estimated to be 178.3 Ω from Fig. 6(b) and ca 10 μm from SEM respectively. The chemical diffusivity of the lithium ion $\tilde{D}_{Li^+}$ was taken as $10^{-8}\,cm^2\,s^{-1}$ from previous work [22]. The electrochemical active area A_{ea} was evaluated to be 24.4 cm^2 for the electrode considered to be composed of the cylindrical particles.

Fig. 7 illustrates on a logarithmic scale the cathodic current transients determined from the numerical solution to Fick's diffusion equations for the conditions of Eqs. (1)–(3) by taking the values described above. The theoretical current transients (Fig. 7) were in good agreement with those obtained experimentally (Fig. 6(a)) in value and shape. It was noteworthy that the theoretical current transient following the potential drop from 4.0 to 3.5 V versus Li/Li^+ showed an almost 'current plateau' after about 4000 s, which results necessarily during the 'potential plateau' interval at 3.65 V versus Li/Li^+ (Fig. 5).

This 'current plateau', however, did not appear in the experimental current transient from 4.0 to 3.5 V versus Li/Li^+. The experimental transient began to show a 'current plateau' only after 8000 s. This implies that lithium intercalation is being extremely retarded. It has been reported [22–24] from impedance studies of $Li_{1-\delta}NiO_2$ that the resistance corresponding to the medium-frequency semicircle in the Nyquist plot increases abruptly at the potential below 3.7 V versus Li/Li^+. So, it is conceivable that lithium intercalation at the low lithium injection potential is impeded by the increased 'cell impedance'.

The retarding effect of 'cell impedance' on lithium intercalation/deintercalation was observed more clearly in the anodic current transient. In Fig. 8(a), none of the anodic current transients showed Cottrell behaviour during the whole lithium deintercalation. In contrast to the cathodic current transient, it is surprising to note that the current even increases rather than decreases

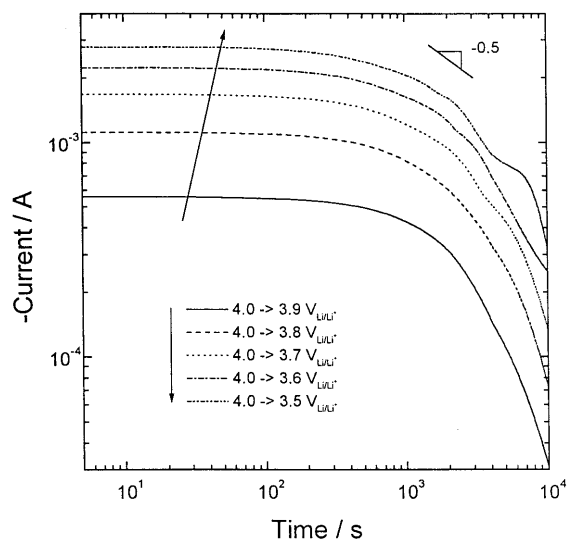

Fig. 7. The cathodic current transients at the potential drops from 4.0 V versus Li/Li^+ to various lithium injection potentials, determined theoretically by numerical analysis based upon the 'cell-impedance-controlled' constraint at the interface between the electrolyte and the electrode of cylindrical symmetry, and the impermeable constraint on the central axis of the cylindrical particle of the electrode.

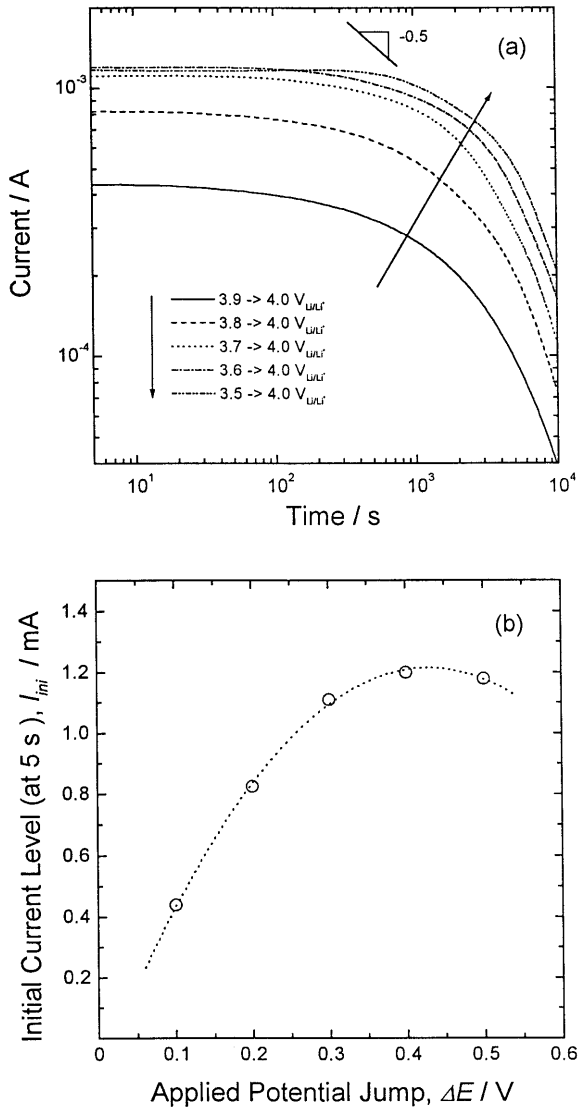

Fig. 8. (a) The anodic current transients obtained experimentally from the $Li_{1-\delta}NiO_2$ electrode in 1 M $LiClO_4$–PC solution at the potential jumps from various initial potentials to 4.0 V versus Li/Li^+, and (b) the dependence of initial current level on applied potential jump.

with time to 200 s in the current transient at the potential jump from 3.5 to 4.0 V versus Li/Li^+ and the relationship between initial current level and applied potential jump takes the form of a parabola (Fig. 8(b)) rather than a straight line (Fig. 6(b)). This result reveals that lithium deintercalation is more considerably retarded by lowering the initial electrode potential, i.e. increasing 'cell impedance'.

Let us first recognise that a greater difference between the applied potential E_{app} and the electrode potential E helps 'cell-impedance-controlled' lithium transport during lithium intercalation/deintercalation, whereas the higher 'cell impedance' R_{cell} hinders the lithium transport. Since a decrease in $|E-E_{app}|$ is much outweighed by a fall in R_{cell} to produce a net increase in the driving force for 'cell-impedance-controlled' lithium transport, it is plausible to state that the current may even increase with time in the current transient at the potential jump from 3.5 to 4.0 V versus Li/Li^+. Further investigations are needed regarding the quantitative analysis of the current transient from $Li_{1-\delta}NiO_2$ in view of the effect of the variation of the 'cell impedance' with lithium stoichiometry on the current transient.

3.3. $Li_\delta V_2O_5$ electrode

Fig. 9 shows the electrode potentials obtained from the intermittent galvanostatic discharge curve of the carbon-dispersed $Li_\delta V_2O_5$ composite electrode in 1 M $LiClO_4$–PC solution as a function of intercalated lithium content. The electrode potential curve displayed two 'potential plateaux' at the electrode potentials of 3.40 V versus Li/Li^+ in the range $\delta = 0.05$–0.3 and of 3.21 V versus Li/Li^+ in the range $\delta = 0.5$–0.85. The appearance of these plateaux is assigned to the coexistence of two phases in equilibrium (α- and ε-$Li_\delta V_2O_5$ phases at 3.40 V versus Li/Li^+ and ε- and δ-$Li_\delta V_2O_5$ phases at 3.21 V versus Li/Li^+) [25].

Fig. 10(a) exhibits on a logarithmic scale the cathodic current transients obtained experimentally from an $Li_\delta V_2O_5$ composite electrode in 1 M $LiClO_4$–PC solution on dropping the applied potential from 3.45 V versus Li/Li^+ to various lithium injection potentials as

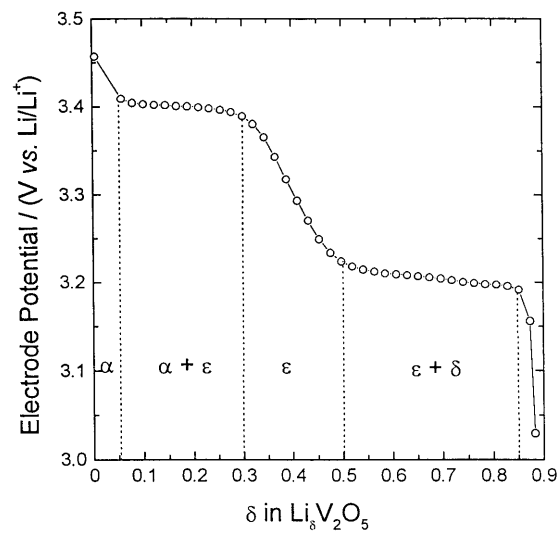

Fig. 9. The intermittent galvanostatic discharge curve obtained from the cell of Li/1 M $LiClO_4$–PC solution/$Li_\delta V_2O_5$. The change in lithium content, $\Delta\delta = 1$, occurs over 10 h.

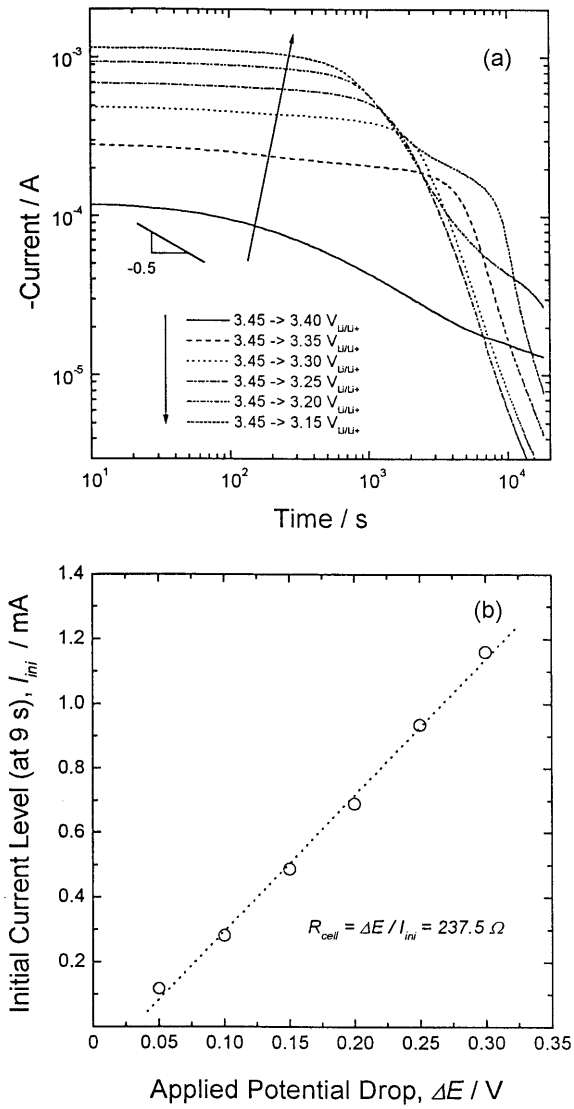

Fig. 10. (a) The cathodic current transients obtained experimentally from the $Li_\delta V_2O_5$ electrode in 1 M $LiClO_4$–PC solution at the potential drops from 3.45 V versus Li/Li^+ to various lithium injection potentials, and (b) the dependence of initial current level on applied potential drop.

indicated in the figure. The shapes of the current transients at the potential drops from 3.45 to 3.40, 3.45 to 3.35, 3.45 to 3.30 and 3.45 to 3.25 V versus Li/Li^+, which passed only through the first plateau potential 3.40 V versus Li/Li^+, were relatively simple: the absolute value of the slope of the logarithmic current transient for the potential drop from 3.45 to 3.40 V versus Li/Li^+ increased monotonically with time to 4000 s, and then decreased. The other transients for 3.45 to 3.35, 3.45 to 3.30 and 3.45 to 3.25 V versus Li/Li^+ showed an almost 'current plateau' before ca 3000 s, 2000 s and 1000 s respectively.

Next, the current transients for the potential drops from 3.45 to 3.20 and 3.45 to 3.15 V versus Li/Li^+, which involved the effect of two 'potential plateaux' at 3.40 and 3.21 V versus Li/Li^+, were characterised by two 'quasi-current-plateau' regions. The first plateau appeared before ca 1000 s and the second after ca 1000 s.

First, it should be mentioned that up to several hundreds of seconds when lithium diffusion was thought to proceed through the single α phase, the Cottrell relation was hardly observed and the initial current–potential relation followed Ohm's law, as can be seen in Fig. 10(b). This indicates that lithium transport occurs in the $Li_\delta V_2O_5$ electrode under the 'cell-impedance-controlled' constraint in the single α phase.

Furthermore, remembering that a 'current plateau' in a current transient indicates 'cell-impedance-controlled' phase transformation, the appearance of the two 'quasi-current plateaux' is attributable to 'cell-impedance-controlled' lithium transport. These results encouraged us to calculate theoretically the current transient under the control of 'cell-impedance' in order to clarify the lithium transport mechanism.

The electrode particle with cylindrical symmetry was chosen for the modelling because of the layered structure of the oxide particle. The 'cell impedance' R_{cell} and the average radius R^* of an oxide particle were determined to be 237.5 Ω from Fig. 10(b) and ca 10 μm from SEM respectively. The chemical diffusivity of the lithium ion $\tilde{D}_{Li^+}$ was taken as $10^{-8}\,cm^2\,s^{-1}$ from previous work [26]. The electrochemically active area A_{ea} was evaluated to be 8.8 cm^2 for the electrode consisting of the cylindrical particles.

Fig. 11 shows on a logarithmic scale the cathodic current transients determined from the numerical solution to Fick's diffusion equations for the conditions of Eqs. (1)–(3) by taking the values described above. The simulated current transients (Fig. 11) coincided fairly well with those determined experimentally (Fig. 10(a)). From these results, it is obvious that lithium transport through a $Li_\delta V_2O_5$ composite electrode in 1 M $LiClO_4$–PC solution is governed purely by 'cell impedance'.

It is noted that the two 'quasi-current-plateaux' in the theoretical current transients appear more clearly compared with those in the experimental current transients. The most plausible reasons for this slight discrepancy are the size distribution of the oxide particles and the variation of 'cell impedance' with lithium stoichiometry. For a more exact quantitative analysis of the current transients, the effects of these factors should be considered.

4. Conclusions

In the present work, the lithium transport mechanisms through such transition metal oxides as $Li_{1+\delta}[Ti_{5/3}Li_{1/3}]O_4$, $Li_{1-\delta}NiO_2$ and $Li_\delta V_2O_5$ have been explained in terms of 'cell-impedance-controlled' intercalation/deintercalation by comparing current transients measured experimentally with those calculated theoretically. The results are summarised as follows.

(1) The experimental current transients scarcely showed Cottrell behaviour during lithium intercalation/deintercalation in a single-phase region. In addition, the relation between the initial current level and the applied potential step followed Ohm's law.

(2) The experimental current transients during the lithium intercalation into two coexisting phases were characterised by 'current plateaux'. This indicates that the driving force for phase transformation from an Li-poor phase to an Li-rich phase remains constant during the lithium intercalation, and hence phase transformation does not occur by a 'diffusion-controlled' process.

(3) The current transients have been simulated as a function of applied potential, based upon the interface between the electrolyte and the electrodes of spherical and cylindrical symmetry subjected to the constraint of 'cell-impedance-controlled' lithium intercalation/deintercalation. The quantitative coincidence of the experimental current transients with those simulated numerically strongly suggests that lithium transport through $Li_{1+\delta}[Ti_{5/3}Li_{1/3}]O_4$, $Li_{1-\delta}NiO_2$ and $Li_\delta V_2O_5$ is controlled purely by 'cell impedance'.

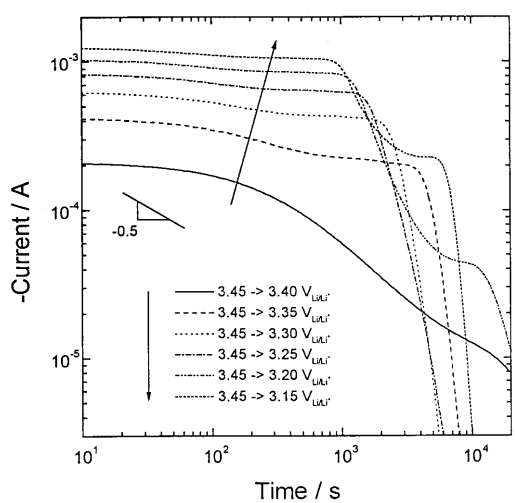

Fig. 11. The cathodic current transients at the potential drops from 3.45 V versus Li/Li^+ to various lithium injection potentials, determined theoretically by numerical analysis based upon the 'cell-impedance-controlled' constraint at the interface between the electrolyte and the electrode of cylindrical symmetry, and the impermeable constraint on the central axis of the cylindrical particle of the electrode.

Acknowledgements

The receipt of a research grant under the programme 'Development of technology of high performance batteries for electric vehicle application 1999/2000' from the Ministry of Commerce, Industry and Energy, Korea, is gratefully acknowledged. Incidentally, this work was supported in the period of 1998/1999 by the Korea Science and Engineering Foundation (KOSEF) through the Center for Interface Science and Engineering of Materials at Korea Advanced Institute of Science and Technology (KAIST). This work was partly supported by the Brain Korea 21 project.

References

[1] M.S. Whittingham, J. Electrochem. Soc. 123 (1976) 315.
[2] D.W. Murphy, P.A. Christian, Science 205 (1979) 651.
[3] K. Mizushima, P.C. Jones, P.J. Wiseman, J.B. Goodenough, Mater. Res. Bull. 15 (1980) 783.
[4] J.R. Dahn, U. von Sacken, C.A. Michal, Solid State Ionics 44 (1990) 87.
[5] O. Bohnke, B. Vuillemin, C. Gabrielli, M. Keddam, H. Perrot, H. Takenouti, R. Torresi, Electrochim. Acta 40 (1995) 2755.
[6] A.J. Vaccaro, T. Palanisamy, R.L. Kerr, J.T. Maloy, J. Electrochem. Soc. 129 (1982) 682.
[7] N. Kumagai, I. Ishiyama, K. Tanno, J. Power Sources 20 (1987) 193.
[8] H.-C. Shin, S.-I. Pyun, Electrochim. Acta. 45 (1999) 489.
[9] S.-I. Pyun, H.-C. Shin, Mol. Cryst. Liq. Cryst. 341 (2000) 147.
[10] S.-I. Pyun, S.-W. Kim, H.-C. Shin, J. Power Sources 81-82 (1999) 248.
[11] Y.-M. Choi, S.-I. Pyun, J.-S. Bae, S.-I. Moon, J. Power Sources 56 (1995) 25.
[12] S.-I. Pyun, J.-S. Bae, Electrochim. Acta 41 (1996) 919.
[13] S. Bach, J.P. Pereira-Ramos, N. Baffier, J. Power Sources 81–82 (1999) 273.
[14] T. Ohzuku, A. Ueda, N. Yamamoto, J. Electrochem. Soc. 142 (1995) 1431.
[15] M.G.S.R. Thomas, P.G. Bruce, J.B. Goodenough, J. Electrochem. Soc. 132 (1985) 1521.
[16] M.G.S.R. Thomas, P.G. Bruce, J.B. Goodenough, Solid State Ionics 17 (1985) 13.
[17] J. Crank, The Mathematics of Diffusion, Clarendon Press, Oxford, 1975, pp. 4, 17.
[18] K. Zaghib, M. Simoneau, M. Armand, M. Gauthier, J. Power Sources 81-82 (1999) 300.
[19] T. Yamamoto, S. Kikkawa, M. Koizumi, Solid State Ionics 17 (1985) 63.
[20] A.J. Bard, L.R. Faulkner, Electrochemical Methods, Wiley, New York, 1980, p. 142.

[21] W. Li, J.N. Reimers, J.R. Dahn, Solid State Ionics 67 (1993) 123.
[22] Y.-M. Choi, S.-I. Pyun, S.-I. Moon, Solid State Ionics 89 (1996) 43.
[23] S. Yamada, M. Fujiwara, M. Kanda, J. Power Sources 54 (1995) 209.
[24] D. Aurbach, M.D. Levi, E. Levi, H. Teller, B. Markovsky, G. Salitra, J. Electrochem. Soc. 145 (1998) 3024.
[25] J.M. Cossinatelli, J.P. Diumerc, M. Pouchard, M. Broussely, J. Labat, J. Power Sources 34 (1991) 101.
[26] P.G. Dickens, G.J. Reynolds, Solid State Ionics 5 (1981) 331.